Structures of Apo- and Holo-Tyrosine Phenol-lyase Reveal a Catalytically Critical Closed Conformation and Suggest a Mechanism for Activation by K^+ Ions[†,‡]

Dalibor Milić,*[,§] Dubravka Matković-Čalogović,[§] Tatyana V. Demidkina,[||] Vitalia V. Kulikova,[||] Nina I. Sinitzina,[||] and Alfred A. Antson[⊥]

Department of Chemistry, Faculty of Science, University of Zagreb, Horvatovac 102a, HR-10000 Zagreb, Croatia, Engelhardt Institute of Molecular Biology, Russian Academy of Sciences, 32 Vavilov Street, Moscow 119991, Russia, and Department of Chemistry, University of York, Heslington, York YO10 5YW, U.K.

Received January 27, 2006; Revised Manuscript Received April 22, 2006

ABSTRACT: Tyrosine phenol-lyase, a tetrameric pyridoxal 5′-phosphate dependent enzyme, catalyzes the reversible hydrolytic cleavage of L-tyrosine to phenol and ammonium pyruvate. Here we describe the crystal structure of the *Citrobacter freundii* holoenzyme at 1.9 Å resolution. The structure reveals a network of protein interactions with the cofactor, pyridoxal 5′-phosphate, and details of coordination of the catalytically important K^+ ion. We also present the structure of the apoenzyme at 1.85 Å resolution. Both structures were determined using crystals grown at pH 8.0, which is close to the pH of the maximal enzymatic activity (8.2). Comparison of the apoenzyme structure with the one previously determined at pH 6.0 reveals significant differences. The data suggest that the decrease of the enzymatic activity at pH 6.0 may be caused by conformational changes in the active site residues Tyr71, Tyr291, and Arg381 and in the monovalent cation binding residue Glu69. Moreover, at pH 8.0 we observe two different active site conformations: open, which was characterized before, and closed, which is observed for the first time in β-eliminating lyases. In the closed conformation a significant part of the small domain undergoes an extraordinary motion of up to 12 Å toward the large domain, closing the active site cleft and bringing the catalytically important Arg381 and Phe448 into the active site. The closed conformation allows rationalization of the results of previous mutational studies and suggests that the observed active site closure is critical for the course of the enzymatic reaction and for the enzyme's specificity toward its physiological substrate. Finally, the closed conformation allows us to model keto(imino)quinonoid, the key transition intermediate.

Tyrosine phenol-lyase (TPL,[1] EC 4.1.99.2) belongs to the group of pyridoxal 5′-phosphate (PLP) dependent enzymes which catalyze a variety of reactions during metabolic transformations of amino acids. TPL catalyzes the reversible β-elimination of L-tyrosine to produce phenol and ammonium pyruvate (Scheme 1). In vitro, it also catalyzes the reversible β-elimination (*1*) and β-substitution (*2*) reactions of other β-substituted amino acids. Reversal of the β-elimination reaction (the so-called "synthetic reaction") catalyzed by TPL was used for the one-step synthesis of several derivatives and heterocyclic analogues. These include a potent antitumor drug 2-aza-L-tyrosine synthesized from 3-hydroxypyridine (*3*) and 3,4-dihydroxy-L-phenylalanine (L-DOPA) produced from catechol (*4*).

Scheme 1: Reversible β-Elimination Reaction of L-Tyrosine Catalyzed by TPL

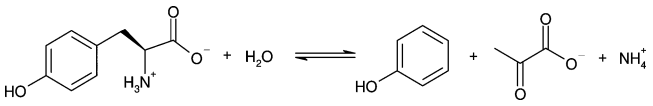

TPL was primarily found in enterobacteria (*5*), but it also occurs in other bacteria and even some arthropods (*6*). Several TPL genes from different bacterial species, including *Escherichia intermedia* (*7*), *Citrobacter freundii* (*8*, *9*), *Enterobacter agglomerans* (*Erwinia herbicola*) (*10*, *11*), *Symbiobacterium thermophilum* (*12*), *Pasteurella multocida* (*13*), *Fusobacterium nucleatum* (*14*), and *Clostridium tetani* (*15*), were cloned, and the primary structures were deduced from the DNA sequences. All of them are highly similar with the sequence identities above 60%.

The three-dimensional structures of TPL from *C. freundii* and *E. herbicola* were established by previous X-ray studies (*9*, *16*, *17*). Each active site of TPL is built up of residues

[†] This work was supported by a grant from the Ministry of Science, Education, and Sports of the Republic of Croatia (0119632) to D.M. and D.M.-Č., by a Wellcome Trust fellowship to A.A.A. (ref. 067416), by an International Fogarty Foundation grant (1 R03 TW006045-01A2), and by a grant from the Russian Foundation for Basic Researchers (05-04-48521) to T.V.D., V.V.K., and N.I.S.

[‡] Coordinates and structure factors of holoTPL and apoTPL were deposited with the RCSB Protein Data Bank with accession numbers 2EZ1 and 2EZ2, respectively.

* To whom correspondence should be addressed. Telephone: +385 1 460 6377. Fax: +385 1 460 6341. E-mail: dmilic@chem.pmf.hr.

[§] University of Zagreb.

[||] Russian Academy of Sciences.

[⊥] University of York.

[1] Abbreviations: apoTPL, apo form of tyrosine phenol-lyase in complex with phosphate at pH 8.0; AspAT, aspartate aminotransferase; holoTPL, holo form of tyrosine phenol-lyase in complex with pyridoxal 5′-phosphate at pH 8.0; rms, root mean square; PLP, pyridoxal 5′-phosphate; TPL, tyrosine phenol-lyase (EC 4.1.99.2); Trpase, tryptophan indole-lyase (tryptophanase) (EC 4.1.99.1).

10.1021/bi0601858 CCC: $33.50
Published on Web 05/24/2006

Scheme 2: Reaction Mechanism of β-Elimination of L-Tyrosine Catalyzed by TPL

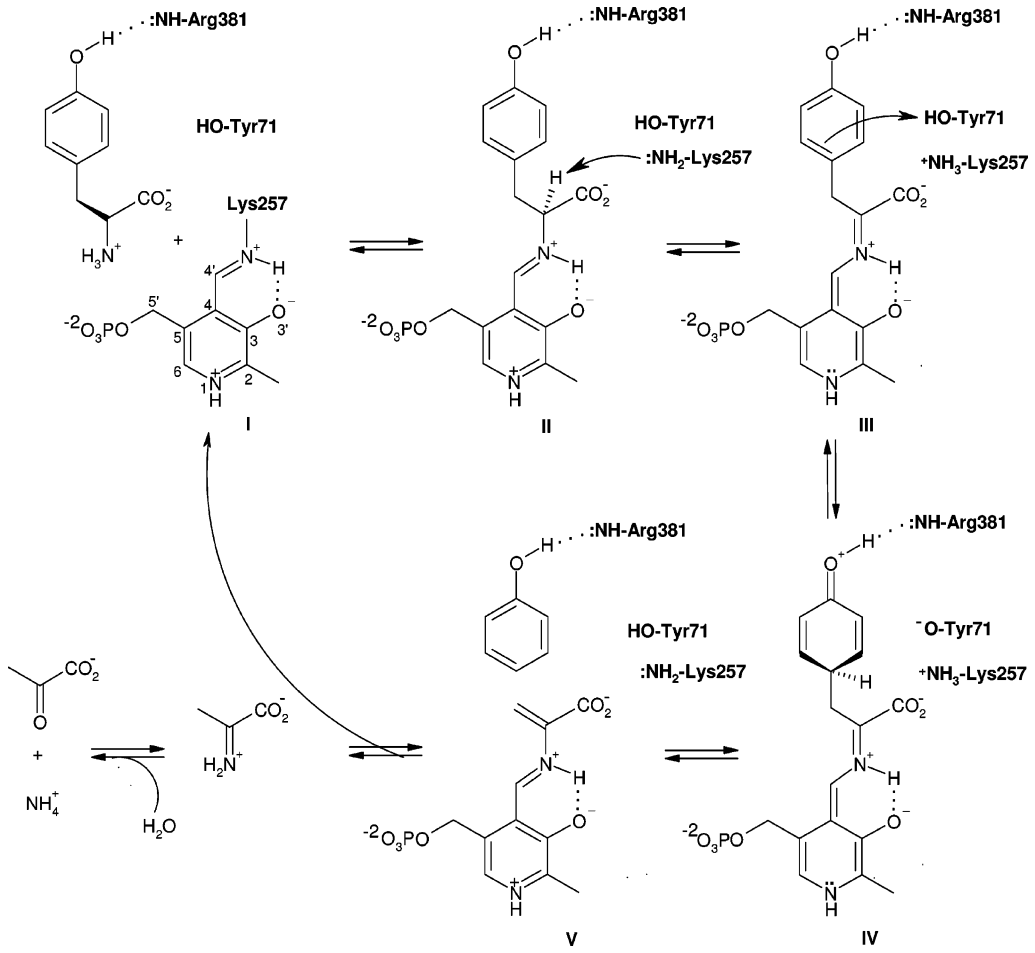

from two subunits that make up a "catalytic dimer". The large domain of each subunit has a characteristic PLP-binding fold, first identified in aspartate aminotransferase (*18*, *19*). Two catalytic dimers are bound through a hydrophobic cluster and intertwined N-terminal arms to form a tetramer. Dimers of that kind, where each subunit contains a large, PLP-binding domain with the characteristic fold and where each active site is composed of residues from both subunits, have been identified in a number of PLP-dependent enzymes including AspAT, which has one such dimer per protein molecule.

The proposed mechanism of β-elimination catalyzed by TPL is shown in Scheme 2 (*20*). It includes the following main steps: formation of the external aldimine with the substrate (**II**), abstraction of the Cα proton of the substrate yielding the quinonoid intermediate (**III**), protonation of Cγ and cleavage of the C−C bond, resulting in the removal of phenol and formation of the aminoacrylate intermediate (**V**). The latter is attacked further by the ϵ-amino group of the active site lysine residue that binds the coenzyme (Lys257), resulting in regeneration of the holoenzyme. The role of several amino acids in the catalysis has been studied by site-directed mutagenesis. It was demonstrated that Asn185 takes part in substrate binding as well as in the catalysis through stabilization of the quinonoid intermediate and possibly also the keto(imino)quinonoid intermediate (**IV**) (*21*). It was also shown that Tyr71 is important for the removal of phenol with the Tyr71 OH group playing the role of the general acid catalyst during the formation of the key transition structure, the keto(imino)quinonoid intermediate (*22*, *23*). Investigations of β-elimination activities of mutant enzymes performed with physiological substrate indicated that Arg381 assists in abstraction of a proton from the phenol hydroxyl group (*16*). In addition, Thr124 and Phe448 were shown to be the residues providing substrate specificity of the enzyme (*24*).

Domain closure was identified in a number of enzymes including AspAT (*25*). The small domain of AspAT rotates during the substrate binding by 13° relative to the large domain. This closure buries the substrate in the active site and reorients the two Arg side chains in order to form salt bridges with the substrate carboxylate groups, thus moving the substrate into the optimal position for the transamination reaction. All domain movements are a consequence of coordinated small structural changes, and only a few side chains change their conformations. In the previously determined structures of TPL and the related β-eliminating lyase, tryptophanase (Trpase), all subunits were in the open conformation.

Here we present the structures of *C. freundii* TPL holo- and apoenzyme in complex with K^+, determined at 1.90 and 1.85 Å resolution, respectively. The previous *C. freundii* TPL apoenzyme structure (PDB ID 1TPL) (*9*) was determined at a lower resolution (2.3 Å) using data obtained from crystals grown at pH 6.0. The apo- and holoenzyme structures presented here were determined from the crystals grown at pH 8.0, which is close to a pH of 8.2 where TPL has maximum activity (*26*). There are significant differences

between the two structures that may account for the considerably lower enzymatic activity at pH 6.0. In the new apoenzyme structure, two different conformations of protein subunits are observed, resulting in open and closed active site conformations. Results of previous mutational studies allow us to propose that the observed active site closure is critical for the course of the enzymatic reaction. We also present a model for a key transition intermediate, keto-(imino)quinonoid.

MATERIALS AND METHODS

Crystallization. TPL was purified from *Escherichia coli* SVS 370 cells containing the plasmid pTZTPL with the gene of the enzyme (*9*). Cells were grown, and the enzyme was purified as described before (*22*). Both TPL apo- and holoenzymes were crystallized at 277 and 293 K using the hanging drop vapor diffusion method. Prior to crystallization, the purified apoenzyme was dialyzed against 50 mM triethanolamine buffer (pH 8.0) containing 2 mM dithiothreitol (DTT) and concentrated using a 30K ultrafiltration membrane concentrator (Filtron) to 18−20 mg/mL. The same procedure was applied for the holoenzyme except that the holoenzyme was dialyzed against the solution that also contained 0.5 mM PLP. For crystallization 2 μL aliquots of the protein solution were mixed on siliconized glass coverslips with an equal volume of the reservoir solution. The reservoir solution for the apoenzyme crystallization contained 50 mM potassium phosphate (pH 8.0), 2 mM DTT, 0.2 M KCl, and 32.5% (w/v) of M_r 2000 monomethyl ether poly(ethylene) glycol (*27*). The crystals of the holoenzyme were grown from 50 mM triethanolamine buffer (pH 8.0), containing 0.5 mM PLP, 2 mM DTT, 0.4−0.8 M KCl, and 35−38% (w/v) of M_r 5000 monomethyl ether poly(ethylene) glycol. Platelike crystals $0.1 \times 0.5 \times 0.5$ mm^3 in size grew within 2 weeks. The combination of KCl and high molecular weight PEG appeared to be a good cryoprotectant and allowed the freezing of TPL crystals directly from the crystallization drops.

X-ray Data Collection. Both diffraction data sets were collected at 120 K. Data for the holoenzyme were collected at the BW7B beamline (EMBL, Hamburg) using a wavelength of 0.87 Å and the 300 mm MarResearch image-plate detector, while the data for the TPL apoenzyme were collected at the BM14 beamline (ESRF, Grenoble) using a wavelength of 1.0 Å and the MarResearh CCD detector. Data sets were processed using DENZO and SCALEPACK (*28*). The main characteristics of the data sets are given in Table 1.

Structure Determination and Refinement. All crystallographic calculations were performed using the CCP4 program package (*29*). Molecular replacement calculations were done with AMoRe (*30*). The initial molecular replacement model for the holoenzyme structure was the structure of the TPL apoenzyme previously determined (PDB ID 1TPL) from crystals obtained with different crystallization conditions (*9*). Rebuilding of the holoenzyme structure was performed with the program FRODO (*31*) running on an Evans and Sutherland ESV series workstation using Fourier syntheses based on the coefficients $(2|F_o| - |F_c|) \exp(i\varphi_c)$ and $(3|F_o| - |F_c|) \exp(i\varphi_c)$. During the later stages, rebuilding was performed with the module XFIT (*32*) in QUANTA (Molecular Simulations Inc.) using Fourier maps with likelihood weighted $2|F_o| - |F_c|$ coefficients. Initial refinement of the holoenzyme model was performed using restrained least-squares minimization (*33*) with individual isotropic atomic displacement parameters, without the use of noncrystallographic symmetry restraints. The last rounds of the holoenzyme model refinement and the refinement of TPL apoenzyme were done with REFMAC5 (*34*) including the TLS refinement (*35*) with the small and the large domain of each subunit as a separate TLS group. Water molecules were added using ARP/wARP (*36*). Additional rebuilding of the TPL apoenzyme model was performed in COOT (*37*). The structures were validated using PROCHECK (*38*), and differences in geometrical parameters of the compared structures were determined using LSQMAN (*39*). The reaction intermediates were docked in the apoTPL active sites using GOLD (*40*, *41*). All structural figures were made by PyMol (*42*).

Table 1: Crystallographic Data Collection and Refinement Statistics

	holoTPL	apoTPL
space group	$P2_12_12$	$P2_12_12$
unit cell parameters		
a (Å)	133.86	133.64
b (Å)	143.85	143.74
c (Å)	60.07	59.92
resolution (Å)	20.00−1.90 (1.95−1.90)[a]	17.00−1.85 (1.90−1.85)
no. of unique reflections[b]	85710 (4151)	95091 (4208)
data redundancy[b]	3.2 (2.0)	3.4 (1.4)
completeness (%)[b]	92.1 (90.7)	95.5 (85.1)
R_{merge}[b] (%)	7.5 (35.9)	5.5 (38.1)
average $I/\sigma(I)$[b]	15.4 (3.6)	19.3 (2.8)
Wilson *B*-factor (Å^2)	28.5	31.0
R_{work} (%)	15.2 (18.5)	17.4 (22.2)
R_{free} (%)	18.6 (24.5)	20.6 (30.7)
no. of reflections used for R_{free}	2508 (3% of total)	939 (1% of total)
no. of residues	910	912
no. of protein atoms	7184	7233
no. of ligands	4 ($2K^+$ and 2PLP)	4 ($2K^+$ and $2PO_4^{3-}$)
no. of water molecules	902	1021
average *B*-factor (Å^2)		
chain A	24.9	28.1
chain B	24.5	25.0
water molecules	39.2	39.5
overall	26.3	28.1
rms deviations		
bond lengths (Å)	0.014	0.015
bond angles (deg)	1.3	1.4
Ramachandran plot (%)		
most favored	92.4	93.3
additionally allowed	7.2	6.4
generously allowed	0.4	0.1
disallowed	0.0	0.1

[a] Values in parentheses are for the outer resolution shell. [b] The highest resolution shell for X-ray data statistics is 1.93−1.90 Å for holoTPL and 1.88−1.85 Å for apoTPL.

RESULTS AND DISCUSSION

Overall Structure of the TPL Holoenzyme. Crystals of the TPL holoenzyme belong to the orthorhombic space group $P2_12_12$ with $a = 133.9$ Å, $b = 143.9$ Å, and $c = 60.1$ Å. Two subunits of TPL per asymmetric unit of the crystal give a specific volume (V_M) (*43*) of 2.81 Å^3 Da^{-1} and solvent content of 55.9%. The structure was refined to an *R*-factor

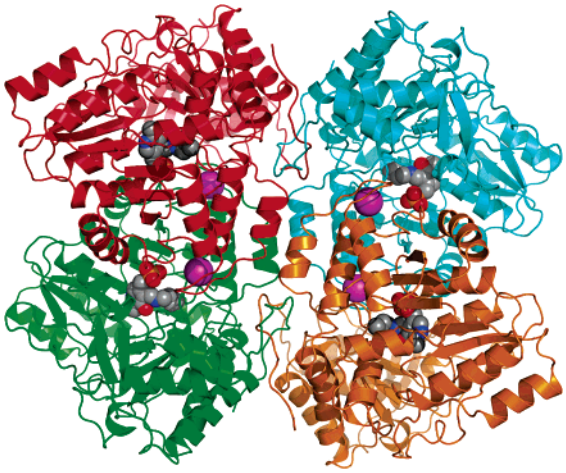

FIGURE 1: Ribbon diagram of the TPL tetramer with different subunits shown in different colors. The PLP, side chains of Lys257, and K^+ ions are shown as spheres. The view is along the crystallographic 2-fold axis.

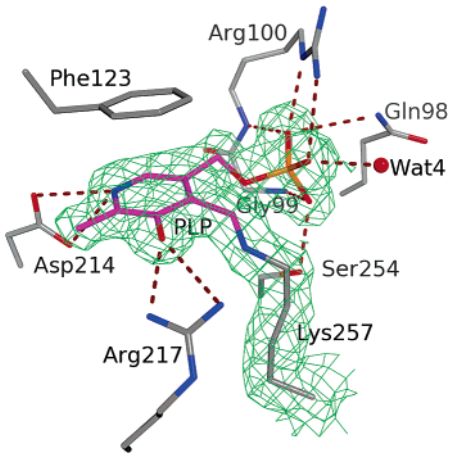

FIGURE 2: Interactions between PLP and the active site residues. Hydrogen bonds are denoted by red dashed lines. The weighted $2|F_o| - |F_c|$ electron density map (green) is contoured at the 1.0σ level.

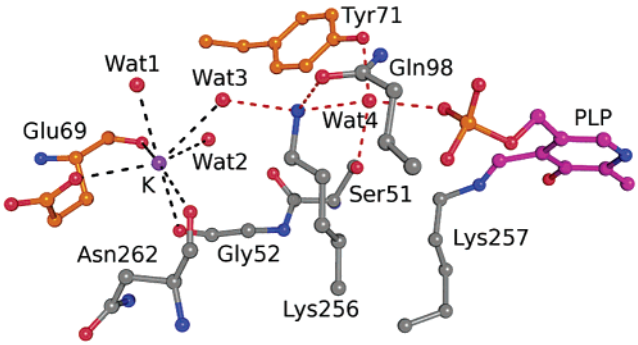

FIGURE 3: The cation-binding site and the active site residues are connected by the hydrogen-bonding interactions. Hydrogen bonds are indicated by red dashed lines. Carbon atoms of residues from the second subunit of the catalytic dimer are shown in orange.

of 15.2% (R_{free} = 18.5%) at 1.9 Å resolution. The final electron density maps allowed the positioning of all residues except for the first N-terminal residues of both subunits (Met1). The final model contains 2 PLP molecules, 2 K^+ ions, and 902 water molecules, giving a total of 8118 atoms. Forty-five atoms of the final model belong to totally disordered protein side chains; these were omitted from the refinement and were given an occupancy of 0. The rest of the model is clearly defined in the electron density maps. The side chains of residues Met66(A), Thr124(A), Glu354-(A), Thr15(B), Met66(B), Ile93(B), and Thr124(B) were modeled in two different conformations with an occupancy of 0.5. None of the non-glycine and non-proline residues lie outside the allowed regions of the Ramachandran plot (*44*).

A PLP molecule is bound in a deep cleft between the small and large domains of each subunit. Two crystallographically independent subunits constitute the so-called catalytic dimer in which each subunit contributes to the active site of the neighboring subunit. The structures of the two subunits are essentially identical, with an average rms deviation between their Cα atoms of only 0.16 Å. Each catalytic dimer contains two K^+ cations, located at the interface between the two subunits. The location of the K^+ cation was confirmed by calculating anomalous difference Fourier maps using phases corresponding to the refined model. As expected for K^+, the coordinating distances are within 2.6−3.8 Å. Two catalytic dimers are related by the crystallographic 2-fold axis generating the TPL tetramer (Figure 1).

Protein Interactions with PLP and K^+. PLP is attached by its C4′ to the Lys257 side chain Nζ via a covalent linkage (Figure 2). The aldimine bond lies in a plane which is rotated 21.1° relative to the PLP plane. The Arg217 side chain is positioned with its guanidinium moiety next to the O3′ atom of the pyridine ring stabilizing its deprotonated state. The negative charge at O3′ in turn stabilizes the protonated form of the imine nitrogen (NH^+) with which it forms a hydrogen bond/salt bridge interaction. In agreement with structural observations, spectral studies of the enzyme in the solution suggest that the TPL internal aldimine exists predominantly in the ketoenamine form with both aldimine and pyridinium nitrogen atoms protonated and with the deprotonated hydroxyl group in the pH range 6.5−8.5 (*45*). The protonated N1 nitrogen of the pyridine ring makes a salt bridge with the side-chain carboxyl oxygen of Asp214. The pyridine ring is above the Thr216 side chain, being stacked against CG2. From the opposite side, the pyridine ring is stacked with the side chain of Phe123 at an angle of 12° to its phenyl ring. The phosphate moiety of PLP forms hydrogen bonds with side-chain atoms of Ser254 and Gln98, the main-chain NH functions of Gly99 and Arg100, and the water molecule Wat4. In addition, the phosphate of PLP makes a salt bridge interaction with the guanidinium group of Arg100. Similar protein−PLP interactions are observed in Trpase (*46*), except for the PLP pyridine ring. Unlike TPL, where the pyridine ring is positioned between phenylalanine and threonine side chains, in Trpase it lies between the side chains of Phe132 and Ala225.

A molecule of TPL binds four potassium cations, one cation per monomer. Each cation is bound at the interface between two crystallographically related subunits stabilizing the structure of the catalytic dimer. It is coordinated by the carbonyl oxygens of Gly52 and Asn262 from one subunit and by the main-chain carbonyl oxygen and side-chain carboxyl oxygens of Glu69 from the adjacent subunit (Figure 3). All of these residues belong to the large domains of protein subunits. Additionally, there are three water molecules completing the coordination sphere of K^+. One of these water molecules forms a hydrogen bond with the amino group of the active site residue Lys256. The amino group

of Lys256 makes additional hydrogen bonds with the carboxamido oxygen of Gln98, also a residue from the active site, and with another water molecule. This water molecule lies in the active site, and it is hydrogen-bonded by the PLP phosphate group and hydroxyl groups from side chains of the active site residues Ser51, Tyr71, and Tyr291 (Figure 3). These concatenated interactions of the cation-binding site with the active site residues demonstrate the critical role of Lys256 in the formation of the monovalent cation binding site in agreement with previous biochemical observations (*47*) and provide an insight into the influence of monovalent cations on the activity of TPL (*48*, *49*). At cation concentrations lower than 100 mM, K^+, NH_4^+, and Rb^+ were shown to be the most effective activators, Cs^+ and Li^+ were significantly less effective, while the effect of Na^+ was negligible. Divalent cations (Mg^{2+}, Ca^{2+}, Ba^{2+}, and Sr^{2+}) did not activate TPL. Different alkaline and earth alkaline cations, because of their different radius to charge ratios, have considerably different coordinations, which explains their different binding abilities to TPL. Differences in coordination of Li^+, K^+, Rb^+, and Cs^+ may cause differences in the cation-binding site conformation and, in turn, slight but key differences in the conformation of the active site.

In the previously determined structure of *C. freundii* TPL complexed with 3-(4′-hydroxyphenyl)propanoate, PLP, and Cs^+ ion (PDB ID 2TPL) (*16*), only one of the two crystallographically independent active sites was occupied by the substrate analogue. In the second site only PLP was bound, so this active site and the nearby cation-binding site (Cs^+) are comparable to those of the holoTPL structure in complex with K^+ reported here. The coordination around Cs^+ is somewhat different from that of K^+ with distances between the metal cation and the coordinating protein atoms being longer by 0.2−0.4 Å. This results in slight changes in the conformation of Cs^+ coordinating residues and also in small changes in the active site conformation. In particular, the hydroxyl of the catalytically critical Tyr71 is 0.16 Å further from the active site than it is in the K^+ structure. We believe these small changes in the active site architecture explain the significant reduction of TPL activity when K^+ is replaced by Cs^+ (*49*) and provide a ground for explaining the role of K^+ in the activation of TPL.

Structurally, the most similar to TPL is tryptophan indole-lyase (Trpase) from *Proteus vulgaris* (*46*), the enzyme which catalyzes the reversible β-elimination reaction of L-tryptophan to form indole and ammonium pyruvate. Trpase and TPL belong to the SCOP family of β-eliminating lyases (*50*). TPL and Trpase from various bacteria show more than 40% overall amino acid sequence identity, with the sequence identity between *C. freundii* TPL and *P. vulgaris* Trpase being 48%. Historically, the important role of monovalent cations in stabilizing the quaternary structure of β-eliminating lyases was best illustrated by the example of *E. coli* Trpase (*51*, *52*). In the absence of PLP and monovalent cations, *E. coli* Trpase reversibly dissociates into two nonactive dimers. As both PLP and the monovalent cation are bound at the subunit−subunit interface of the catalytic dimer, it is likely that the dissociation occurs along this interface. In the available structures of Trpase and TPL the two catalytic dimers are held together by intertwined N-terminal arms (*46*), suggesting that the observed dissociation of the *E. coli* Trpase tetramer leads to noncatalytic dimers where the two subunits are bound through their N-terminal arms. Available data suggest that TPL does not undergo such dissociation in the absence of PLP and monovalent cations, but like in the case of Trpase, its activity is influenced by monovalent cations.

Two Conformations of Apoenzyme Subunits in the Asymmetric Unit. Like holoenzyme, TPL apoenzyme crystallizes in the space group $P2_12_12$ with one catalytic dimer per asymmetric unit. Unit cell parameters (a = 133.6 Å, b = 143.7 Å, c = 59.9 Å) are almost identical to those of the holoenzyme. This structure was refined to an R-factor of 17.4% (R_{free} = 20.6) at 1.85 Å resolution. The final model comprises 8266 atoms, including 1021 water molecules, 2 PO_4^{3-} anions, and 2 K^+ cations. Residues Ser17(A) and Arg9(B) were modeled with two alternate side-chain conformations with occupancies of 0.5. All non-glycine and non-proline residues, except Met121(A), are in the allowed regions of the Ramachandran plot. Met121(A) has very unfavorable main-chain torsion angles (φ = 75.4°, ψ = 143.9°), but its average B-factor is relatively low (31.7 Å^2) and the corresponding electron density unambiguous.

In contrast to the holoenzyme structure with two crystallographically independent subunits being essentially identical, two subunits in the asymmetric unit of the apoenzyme have significantly different conformations. One subunit (denoted B) has the same conformation of its main-chain atoms as the holoenzyme, which is characterized by a deep cleft between the two domains of each subunit. In the second subunit (A) protein domains have different orientation, and the cleft is closed. To describe basic structural changes that produce the domain movements and the closure of the active site, we did two iterative analyses of error-scaled difference distance matrices of several known TPL structures using ESCET (*53*). The initial and preliminary analysis with standard parameters (n_{hyp} = 20, w_p = 20.0, r_{mut} = 5.0%) and lower and upper tolerance levels of ϵ_l = 5.0 and ϵ_h = 10.0 included individual subunits from structures of *C. freundii* TPL apoenzyme at pH 6.0 (PDB ID 1TPL), *C. freundii* TPL complexed with 3-(4′-hydroxyphenyl)propanoate, PLP, and Cs^+ ion at pH 8.0 (PDB ID 2TPL), *E. herbicola* TPL holoenzyme at pH 6.2 (PDB ID 1C7G), and TPL holo- and apoenzyme structures reported here. The pairwise comparison for 386 Cα atoms that are present in all models showed high main-chain conformational uniformity for all subunits of 2TPL, 1C7G, and the holoenzyme. Besides being mutually identical, their main-chain conformations are also practically the same as that of the apoenzyme subunit B (open conformation). In order not to overweight redundant conformers, in subsequent ESCET analysis all of these subunits were represented by the apoenzyme subunit B, the conformer with the lowest mean standard uncertainty (0.10 Å). The ESCET analysis for finding the conformationally invariant regions of TPL also included the apoenzyme subunit A (closed conformation), a conformer substantially different from all others. Two subunits of 1TPL with mutually identical main-chain conformations, although different from other subunits, were excluded from the ESCET analysis for finding the conformationally invariant regions of TPL due to two reasons: (a) the main-chain fold in several protein regions is completely different from that found in other TPL structures (see below), and (b) about 6% of amino acid residues had poor electron density and were not modeled.

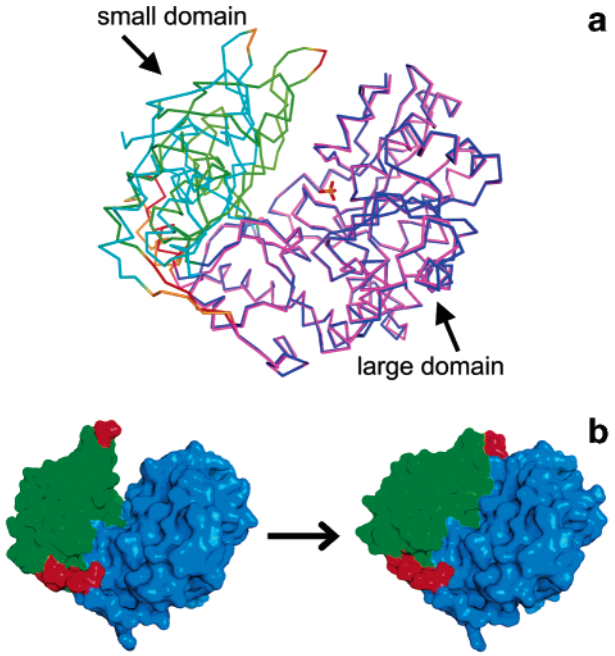

FIGURE 4: (a) Comparison of the open and closed conformations of apoTPL. Two subunits are superimposed using Cα atoms of their large rigid regions. The large and small rigid regions of the subunit in the closed conformation are shown in dark blue and green, respectively, and the flexible parts are shown in red. The large rigid region in the open subunit is shown in magenta, the small rigid region in cyan, and the flexible parts in orange. The position of the active site is indicated by phosphate anions. (b) Structural transition from the open to the closed state. Molecular surfaces of TPL are colored as in the closed conformation in (a).

The ESCET analysis of the apoenzyme subunits A and B, using standard parameters and lower and upper tolerance levels of $\epsilon_l = 5.0$ and $\epsilon_h = 10.0$, detected two conformationally invariant (rigid) regions [large (residues 1−13, 45−345, 405−422) and small (residues 19−44, 346−389, 392−404, 434−456)] and three flexible parts (residues 14−18, 390−391, 423−433) of the apoenzyme TPL subunit (Figure 4). The large rigid region contains almost all of the N-terminal arm (residues 1−13), all of the large domain (residues 57−310), the domain-connecting regions (residues 49−56 and 311−332), and parts of the small domain (residues 45−48, 333−345, and 405−422). The small rigid region is composed exclusively of the residues from the small domain. Two flexible parts (residues 14−18 and 423−433) connect the large and the small rigid regions, while the third flexible part (residues 390 and 391) lies in a loop on the surface of the molecule that comprises residues with higher *B*-factors. Comparison of the open and the closed subunits superimposed by their Cα atoms from the large rigid regions (rms deviation 0.35 Å) reveals structural changes during the active site closure. The closed conformation is achieved by rotation of the small rigid region by about 16° around a hinge connecting the two rigid parts, during which the small rigid region moves toward the large one, with the far end of the small rigid region moving by about 12 Å. The main-chain torsion angles of residues from the flexible parts and some of those found to be at the ends of the rigid regions change considerably upon closure. The extreme examples are Ser17 with $\Delta\varphi$ of −74.3° and $\Delta\psi$ of −170.4° and Met18 with $\Delta\varphi$ of −177.6° and $\Delta\psi$ of 114.0° ($\Delta\varphi$ and $\Delta\psi$ are differences in main-chain torsion angles between the closed and open subunit in the apoenzyme structure).

The closed conformation is stabilized by a number of interactions between the two rigid regions. These include a hydrogen bond/salt bridge between side chains of Arg351-(A) and Asp348(A) and hydrogen bonds Leu38(A) N···Thr35(A) O and Leu38(A) O···Arg377(A) NH1. These interactions are not observed for the equivalent residues of the open subunit (B).

Open vs Closed Active Site. The conformation of the open active site in the apoenzyme is almost identical to the conformation of active sites found in the holoenzyme. In the two forms of the TPL apoenzyme superimposed using the Cα atoms of the large rigid domain of one of the protein subunits, there are only a few minor differences in the position and conformation of the active site residues. One phosphate anion is bound in each active site of the TPL apoenzyme and occupies the same position as the phosphate group of PLP in the active site of the holoenzyme. Thus, all interactions found between the PLP phosphate group and the residues of the holoenzyme active site are also observed in both active sites of the apoenzyme. Additionally, the PO_4^{3-} in the structure of the TPL apoenzyme forms hydrogen bonds with three water molecules and a salt bridge with the side chain of Lys257. As expected, the side-chain conformation of Lys257 changes during cofactor binding and formation of the internal aldimine, as indicated by differences in χ_3 and χ_4 torsion angles of ∼27° and ∼91°, respectively. Another significant difference is in the side-chain conformation of Asn185. The carboxamide group of Asn185 in holoTPL rotates by ∼90° with concomitant change of χ_1 by ∼25°. Also, the side chain of Asp214 moves in order to form a salt bridge with the protonated N1 nitrogen of the PLP pyridine ring. Some minor differences are also observed in side-chain conformations of Met288, Phe123, and Thr124. In addition, the side chain of Thr124 in holoTPL has been found in two alternative conformations related to each other by a rotation around the Cα−Cβ of ∼120°.

The major difference between the closed and the open active sites of the TPL apoenzyme, as expected, is in the position and in the conformation of residues from the small rigid region (Phe36, Met391, Arg381, Arg404, Phe448, Phe449; Figure 5). Phe448 and Phe449 make the largest movement during the active site closure. Differences in the positions of their Cα atoms relative to the large rigid region in the closed and the open forms are 4.9 Å. In addition to the movement of the polypeptide chain, some differences in conformation of the side chains are also observed. The largest difference was found for the phenyl moiety of Phe449 for which χ_1 and χ_2 angles changed by 91.6° and 67.3°, respectively, so in the closed conformation it points toward the interior of the active site. Because of this, the side-chain conformations of Tyr71 and Met288 from the neighboring subunit, that of Phe36 from the small rigid region, and those of Phe123, Thr124, and Asn185 from the large rigid region have also changed. Other residues from the active site go only through minor conformational changes during the active site closure. The closed active site is not completely buried, so it remains accessible to exterior solvent, although the solvent-accessible area of the residues forming the active site cleft is ∼240 Å^2 smaller than in the open form. The conformation of the neighboring monovalent cation-binding

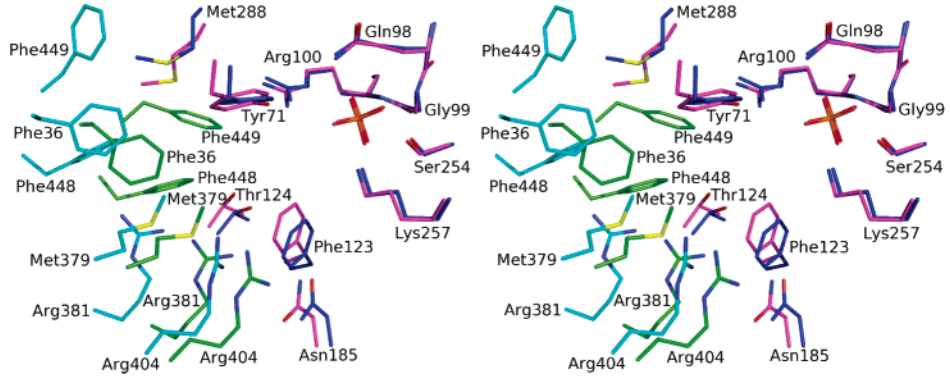

FIGURE 5: Comparison of the two active sites of apoTPL in the catalytic dimer. Residues of the large rigid region from the subunit in the open conformation are shown in magenta, and those of the small rigid region are shown in cyan. In the second subunit, which is in the closed conformation, the corresponding areas are shown in blue and green.

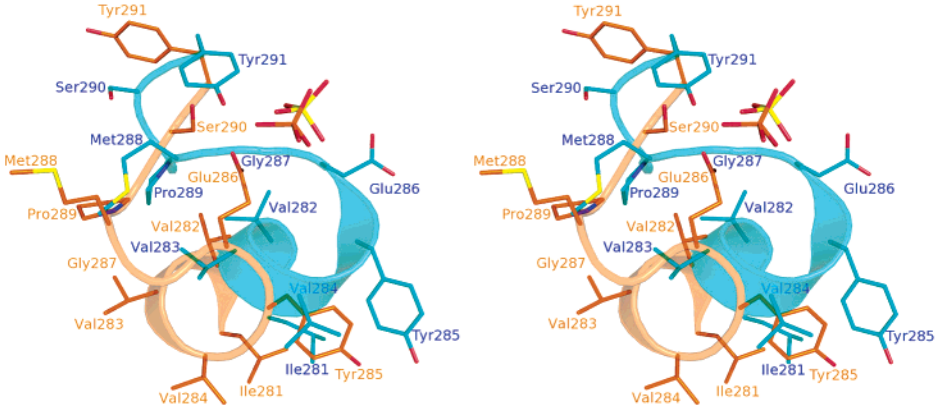

FIGURE 6: Structural comparison of residues 281−291 in 1TPL (orange) and in the previously determined structure of apoTPL at low pH (cyan). A sulfate in 1TPL is bound in the same site as phosphate in the apoTPL.

site, as being formed only by residues from the large rigid regions, remains the same in both conformations.

It is interesting to note that Arg381 and Phe448 are from the small rigid region and during the active site closure they undergo significant conformational changes. The active site Thr124 is in the large rigid region; its conformation remains essentially the same during the closure of the active site.

Differences between TPL Apoenzyme Structures Determined at pH 6.0 and pH 8.0. While the optimum pH for the β-elimination of L-tyrosine is around 8.2, at pH 6.0 the enzyme is essentially inactive (*26*). The differences in the activity of the enzyme at high and low pH were attributed to protonation of two catalytic bases with average pK_a values of about 7.8 (*54*). The side chain of Arg381 was shown to be one of these two bases (*16*), but the identity of the other catalytic base remained uncertain, although the previous structural study suggested it might be the amino group of Lys257 (*16*). Structural data on the closed conformation of the apoenzyme reported here provide further insights about the catalytic residues (see below).

In contrast to the new apoenzyme structure determined from the crystal grown with monomethyl ether poly(ethylene) glycol 2000 at pH 8.0, the previous structure was determined using a different crystal form, with crystals grown at pH 6.0 using ammonium sulfate as a precipitant (*55*). In the previously determined structure (PDB ID 1TPL; 2.3 Å resolution) several stretches of residues were not modeled due to poor electron density: residues 123−131, 384−398, and 442−447 in one subunit and residues 123−133, 384−398, and 442−445 in the crystallographically independent subunit (*9*). Both noncrystallographically related subunits of 1TPL (which do not constitute the catalytic dimer) are very similar to each other and are basically in the open conformation. As major differences between open and closed conformations of TPL subunits have already been described, the structure of 1TPL is only compared with the open conformation. These were found by the ESCET analysis of the corresponding subunits of apoenzyme structures determined previously and described here, using the standard parameters (see above) and lower and upper tolerance levels of $\epsilon_l = 5.0$ and $\epsilon_h = 10.0$. Except for the parts of the 1TPL model with missing residues, ESCET found the difference between the two models in four polypeptide regions: 70−74, 187−188, 281−290, and 382−383. The most striking difference is in the tilt of helix α9 (*9*), where the Cα positions of C-terminal residues 281−285 differ by 1.0−4.7 Å, and in the following active site loop area, residues 286−290, which has a different conformation in the two structures (Figure 6). Despite these major differences in both structures, the active sites remain open. It is reasonable to conclude that the observed different conformations in the previously determined structure of the apoenzyme are due to the difference in the pH (6.0 as opposed to 8.0). In addition, some differences may account for different crystallization conditions (at pH 6.0 crystals were grown with ~1 M ammonium sulfate and kept in 1 M magnesium sulfate during the data collection) and possibly also the radiation damage (as at pH 6.0 the data were collected at room temperature).

Functional Implications. The observed differences in residue segments 70−74, 281−290, and 382−383 between

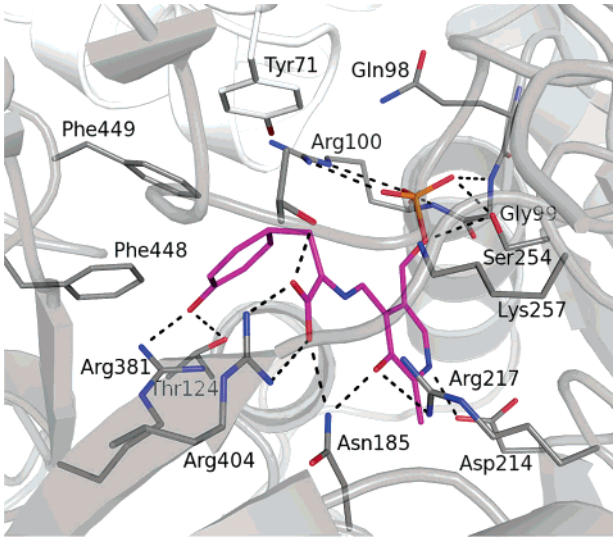

FIGURE 7: Model of the keto(imino)quinonoid form bound in the closed conformation of the TPL active site. Hydrogen bonds (dashed lines) between the hydroxyl group of the keto(imino)quinonoid form and both Thr124 and Arg381 side chains are possible only in the closed conformation, as well as van der Waals contact between the Phe448 phenyl ring and the covalently bound substrate.

structures of the apoenzyme at pH 6.0 and pH 8.0 include changes in conformations of residues participating in the catalysis (Tyr71) and in monovalent cation binding (Glu69). In addition, there are differences in the conformations of the adjacent active site residues Arg381 and Tyr291. These conformational differences, together with the different protonation states of the catalytic bases, may account for the observed significant reduction of TPL activity at pH 6.0 (*26*).

The observed closure of the active site allows us to rationalize the results of previous mutational studies. In the previously determined structure of TPL in complex with the substrate analogue, 3-(4′-hydroxyphenyl)propanoate (*16*), modeling the Michaelis complex, the active site remains in the "open" conformation, with the catalytically important Tyr71, Thr124, and Arg381 being positioned too far from the substrate. Indeed, the phenol hydroxyl of Tyr71 is 3.7 Å from the substrate analogue Cγ, the side chain NH1 of Arg381 and the side chain hydroxyl of Thr124 are 4.1 and 4.9 Å, respectively, from the substrate analogue phenol hydroxyl. Closure of the active site cleft at a stage after Michaelis complex formation, similar to that observed in the present study of the apoenzyme structure, would bring all catalytic residues closer to the catalytic site and thus is likely to favor the catalysis. Indeed, our modeling shows that the keto(imino)quinonoid intermediate (**IV**; Scheme 2) fits best the active site cleft in the closed conformation with the side chains of Thr124 and Arg381 being in the optimal position for forming hydrogen bonds with the hydroxyl group of the substrate. In addition, the van der Waals contact between the Phe448 phenyl ring and the bound substrate is possible only in the closed conformation (Figure 7). In accordance, solvent-accessible areas of Thr124, Arg381, and Phe448 are most affected by the closure of the active site, and in the closed conformation these are decreased by 81, 58, and 31 Å^2, respectively. In our model, Asn185 forms hydrogen bonds with the 3′-hydroxy group of the cofactor and the carboxylic group of the bound substrate, thus, as previously proposed (*21*), stabilizing the keto(imino)quinonoid intermediate. Tyr71 is in a favorable position for proton donation to Cγ of the substrate. In the open conformation its side-chain hydroxyl is interconnected by a net of hydrogen bonds with the side chains of several other residues, including the Lys257, which was proposed to be involved in proton abstraction from the Cα position of the substrate (*20*). This system, involving Lys257−Tyr71, could play the role of one of the two catalytic bases (*54*).

We propose that the closure of the active site observed here is critical for the catalysis as it brings Arg381/Phe448 (small rigid region) and other active site residues into the position suitable for interactions with reaction intermediates and protects them from solvent, thus making the β-elimination of L-Tyr possible and more efficient. To elucidate the exact structural events that occur during the catalysis, further structural studies of TPL complexes with reaction intermediates are needed.

ACKNOWLEDGMENT

We thank Martin Walsh for help during data collection at the BM14 beamline, ESRF, Grenoble. BM14 is supported by the U.K. Research Councils, the BBSRC, the EPSRC, and the MRC. We also thank Robert Byrne for critically reading the manuscript and for useful suggestions.

REFERENCES

1. Yamada, H., and Kumagai, H. (1975) Synthesis of L-tyrosine-related amino acids by β-tyrosinase, *Adv. Appl. Microbiol. 19*, 249−288.
2. Phillips, R. S., Ravichandran, K., and Von Tersch, R. L. (1989) Synthesis of L-tyrosine from phenol and *S*-(*o*-nitrophenyl)-L-cysteine catalysed by tyrosine phenol-lyase, *Enzyme Microb. Technol. 11*, 80−83.
3. Watkins, E. B., and Phillips, R. S. (2001) Enzymatic synthesis of aza-L-tyrosines, *Bioorg. Med. Chem. Lett. 11*, 2099−2100.
4. Lee, S.-G., Ro, H.-S., Hong, S.-P., Kim, E.-H., and Sung, M.-H. (1996) Production of L-DOPA by thermostable tyrosine phenol-lyase of a thermophilic *Symbiobacterium* species overexpressed in recombinant *Escherichia coli*, *J. Microbiol. Biotechnol. 6*, 98−102.
5. Enei, H., Matsui, H., Yamashita, K., Okumura, S., and Yamada, H. (1972) Distribution of tyrosine phenol-lyase in microorganisms, *Agric. Biol. Chem. 37*, 1861−1868.
6. Duffey, S. S., Aldrich, J. R., and Blum, M. S. (1977) Biosynthesis of phenol and guaiacol by the hemipteran *Leptoglossus phyllopus*, *Comp. Biochem. Physiol. B 56*, 101−102.
7. Kurusu, Y., Fukushima, M., Kohama, K., Kobayashi, M., Terasawa, M., Kumagai, H., and Yukawa, H. (1991) Cloning and nucleotide sequencing of the tyrosine phenol-lyase gene from *Escherichia intermedia*, *Biotechnol. Lett. 13*, 762−772.
8. Iwamori, S., Yoshino, S., Ishiwata, K., and Makiguchi, N. (1991) Structure of tyrosine phenol-lyase genes from *Citrobacter freundii* and structural comparison with tryptophanase from *Escherichia coli*, *J. Ferment. Bioeng. 72*, 147−151.
9. Antson, A. A., Demidkina, T. V., Gollnick, P., Dauter, Z., Von Tersh, R. L., Long, J., Berezhnoy, S. N., Phillips, R. S., Harutyunyan, E. H., and Wilson, K. S. (1993) Three-dimensional stucture of tyrosine phenol-lyase, *Biochemistry 32*, 4195−4206.
10. Suzuki, H., Nishihara, K., Usui, N., Matsui, H., and Kumagai, H. (1993) Cloning and nucleotide sequence of *Erwinia herbicola* AJ2982 tyrosine phenol-lyase gene, *J. Ferment. Bioeng. 75*, 145−148.
11. Foor, F., Morin, N., and Bostian, K. (1993) Production of L-dihydroxyphenylalanine in *Escherichia coli* with the tyrosine phenol-lyase gene cloned from *Erwinia herbicola*, *Appl. Environ. Microbiol. 59*, 3070−3075.
12. Hirahara, T., Horinouchi, S., and Beppu, T. (1993) Cloning, nucleotide sequence, and overexpression in *Escherichia coli* of the β-tyrosinase gene from an obligately symbiotic thermophile, *Symbiobacterium thermophilum*, *Appl. Microbiol. Biotechnol. 39*, 341−346.

13. May, B. J., Zhang, Q., Li, L. L., Paustian, M. L., Whittam, T. S., and Kapur, V. (2001) Complete genomic sequence of *Pasteurella multocida* Pm70, *Proc. Natl. Acad. Sci. U.S.A. 98*, 3460−3465.
14. Kapatral, V., Anderson, I., Ivanova, N., Reznik, G., Los, T., Lykidis, A., Bhattacharyya, A., Bartman, A., Gardner, W., Grechkin, G., Zhu, L., Vasieva, O., Chu, L., Kogan, Y., Chaga, O., Goltsman, E., Bernal, A., Larsen N., D'Souza, M., Walunas, T., Pusch, G., Haselkorn, R., Fonstein, M., Kyrpides, N. C., and Overbeek, R. (2002) Genome sequence and analysis of the oral bacterium *Fusobacterium nucleatum* strain ATCC 25586, *J. Bacteriol. 184*, 2005−2018.
15. Brüggemann, H., Bäumer, S., Fricke, W. F., Wiezer, A., Liesegang, H., Decker, I., Herzberg, C., Martinez-Arias, R., Merkl, R., Henne, A., and Gottschalk, G. (2003) The genome sequence of *Clostridium tetani*, the causative agent of tetanus disease, *Proc. Natl. Acad. Sci. U.S.A. 100*, 1316−1321.
16. Sundararaju, B., Antson, A. A., Phillips, R. S., Demidkina, T. V., Barbolina, M. V., Gollnick, P., Dodson, G. G., and Wilson, K. S. (1997) The crystal structure of *Citrobacter freundii* tyrosine phenol-lyase complexed with 3-(4-hydroxyphenyl)propionic acid, together with site-directed mutagensis and kinetic analysis, demonstrated that arginine 381 is required for substrate specificity, *Biochemistry 36*, 6502−6510.
17. Pletnev, S. V., Antson, A. A., Sinitsyna, N. I., Dauter, Z., Isupov, M. N., Hurs, E. N., Faleev, N. G., Wilson, K. S., Dodson, G., Demidkina, T. V., and Arutyunyan, E. G. (1997) Crystallographic study of tyrosine phenol-lyase from *Erwinia herbicola*, *Crystallogr. Rep. 42*, 809−819.
18. Ford, G. C., Eichele, G., and Jansonius, J. N. (1980) Three-dimensional structure of a pyridoxal-phosphate-dependent enzyme, mitochondrial aspartate aminotransferase, *Proc. Natl. Acad. Sci. U.S.A. 77*, 2559−2563.
19. Borisov, V. V., Borisova, S. N., Sosfenov, N. I., and Vainshtein, B. K. (1980) Electron density map of chicken heart cytosol aspartate transaminase at 3.5 Å resolution, *Nature 284*, 189−190.
20. Phillips, S. R., Demidkina, T. V., and Faleev, N. G. (2003) Structure and mechanism of tryptophan indole-lyase and tyrosine phenol-lyase, *Biochim. Biophys. Acta 1647*, 167−172.
21. Barbolina, M. V., Phillips, R. S., Gollnick, P. D., Faleev, N. G., and Demidkina, T. V. (2000) *Citrobacter freundii* tyrosine phenol-lyase: the role of asparagine 185 in modulating of enzyme function through stabilization of quinonoid intermediate, *Protein Eng. 13*, 207−215.
22. Chen, H. Y., Demidkina, T. V., and Phillips, R. S. (1995) Site-directed mutagenesis of tyrosine-71 to phenylalanine in *Citrobacter freundii* tyrosine phenol-lyase: evidence for dual roles of tyrosine-71 as a general acid catalyst in the reaction mechanism and in cofactor binding, *Biochemistry 34*, 12276−12283.
23. Phillips, R. S., Johnson, N., and Kamath, A. V. (2002) Formation in vitro of hybrid dimers of H463F and Y74F mutant *Escherichia coli* tryptophan indole-lyase rescues activity with L-tryptophan, *Biochemistry 41*, 4012−4019.
24. Demidkina, T. V., Barbolina, M. V., Faleev, N. G., Sundararaju, B., Gollnick, P. D., and Phillips, R. S. (2002) Threonine-124 and phenylalanine-448 in *Citrobacter freundii* tyrosine phenol-lyase are necessary for activity with L-tyrosine, *Biochem. J. 363*, 745−752.
25. McPhalen, C. A., Vincent, M. G., Picot, D., Jansonius, J. N., Lesk, A. M., and Chothia, C. (1992) Domain closure in mitochondral aspartate aminotransferase, *J. Mol. Biol. 227*, 197−213.
26. Kumagai, H., Yamada, H., Matsui, H., Ohkishi, H., and Ogata, K. (1970) Tyrosine phenol lyase. I. Purification, crystallization, and properties, *J. Biol. Chem. 245*, 1767−1772.
27. Brzozowski, A. M., and Tolley, S. P. (1994) Poly(ethylene) glycol monomethyl ethers—an alternative to poly(ethylene) glycols in protein crystallization, *Acta Crystallogr., Sect. D 50*, 466−468.
28. Otwinowski, Z., and Minor, W. (1997) Processing of X-ray diffraction data collected in oscillation mode, *Methods Enzymol. 276*, 307−326.
29. Collaborative Computational Project, Number 4 (1994) The CCP4 Suite: Programs for Protein Crystallography, *Acta Crystallogr., Sect. D 50*, 760−763.
30. Navaza, J. (1994) *AMoRe*: an automated package for molecular replacement, *Acta Crystallogr., Sect. A 50*, 157−163.
31. Jones, T. A. (1985) Interactive computer graphics: FRODO, *Methods Enzymol. 115*, 157−171.
32. Oldfield, T. J. (1994) A semi-automated map fitting procedure, in *Proceedings of the CCP4 Study Weekend* (Bailey, S., Hubbard, R., and Waller, D., Eds.) SRS Daresbury Laboratory, Warrington, U.K.
33. Hendrickson, W. A., and Konnert, J. H. (1980) in *Computing in Crystallography* (Diamond, R., Ramaseshan, S., and Venkatesan, K., Eds.) Chapter 13, pp 13.01−13.26, Indian Academy of Sciences, Bangalore.
34. Murshudov, G. N., Vagin, A. A., and Dodson, E. J. (1997) Refinement of macromolecular structures by the maximum-likelihood method, *Acta Crysallogr., Sect. D 53*, 240−255.
35. Winn, M. D., Isupov, M. N., and Murshudov, G. N. (2001) Use of TLS parameters to model anisotropic displacements in macromolecular refinement, *Acta Crystallogr., Sect. D 57*, 122−133.
36. Perrakis, A., Morris, R., and Lamzin, V. S. (1999) Automated protein model building combined with iterative structure refinement, *Nat. Struct. Biol. 6*, 458−463.
37. Emsley, P., and Cowtan, K. (2004) Coot: model-building tools for molecular graphics, *Acta Crystallogr., Sect. D 60*, 2126−2132.
38. Laskowski, R. A., MacArthur, M. W., Moss, D. S., and Thornton, J. M. (1993) PROCHECK: a program to check the stereochemical quality of protein structures, *J. Appl. Crystallogr. 26*, 283−291.
39. Kleywegt, G. J. (1996) Use of non-crystallographic symmetry in protein structure refinement, *Acta Crystallogr., Sect. D 52*, 842−857.
40. Jones, G., Willett, P., Glen, R. C., Leach, A. R., and Taylor, R. (1997) Development and validation of a genetic algorithm for flexible docking, *J. Mol. Biol. 267*, 727−748.
41. Verdonk, M. L., Cole, J. C., Hartshorn, M. J., Murray, C. W., and Taylor, R. D. (2003) Improved protein−ligand docking using GOLD, *Proteins 52*, 609−623.
42. DeLano, W. L. (2002) The PyMOL Molecular Graphics System, DeLano Scientific, San Carlos, CA (http://www.pymol.org).
43. Matthews, B. W. (1968) Solvent content of protein crystals, *J. Mol. Biol. 33*, 491−497.
44. Ramakrishnan, C., and Ramachandran, G. N. (1965) Stereochemical criteria for polypeptide and protein chain conformations. II. Allowed conformations for a pair of peptide units, *Biophys. J. 5*, 909−933.
45. Bazhulina, N. P., Morozov, Y. V., Papisova, A. I., and Demidkina, T. V. (2000) Pyridoxal 5′-phosphate Schiff base in *Citrobacter freundii* tyrosine phenol-lyase. Ionic and tautomeric equilibria, *Eur. J. Biochem. 267*, 1830−1836.
46. Isupov, M. N., Antson, A. A., Dodson, E. J., Dodson, G. G., Dementieva, I. S., Zakomirdina, L N., Wilson, K. S., Dauter, Z., Lebedev, A. A., and Harutyunyan, E. H. (1998) Crystal structure of tryptophanase, *J. Mol. Biol. 276*, 603−623.
47. Phillips, R. S., Chen, H. Y., Shim, D., Lima, S., Tavakoli, K., and Sundararaju, B. (2004) Role of lysine-256 in *Citrobacter freundii* tyrosine phenol-lyase in monovalent cation activation, *Biochemistry 43*, 14412−14419.
48. Sundararaju, B., Chen, H., Shilcutt, S., and Phillips, R. S. (2000) The role of glutamic acid-69 in the activation of *Citrobacter freundii* tyrosine phenol-lyase by monovalent cations, *Biochemistry 39*, 8546−8555.
49. Demidkina, T. V., and Myagkikh, I. V. (1989) The activity and reaction specificity of tyrosine phenol-lyase regulated by monovalent cations, *Biochimie 71*, 565−571.
50. Murzin, A. G., Brenner, S. E., Hubbard, T., and Chothia, C. (1995) SCOP: a structural classification of proteins database for the investigation of sequences and structures, *J. Mol. Biol. 247*, 536−540.
51. Suelter, C. H., and Snell, E. E. (1977) Monovalent cation activation of tryptophanase, *J. Biol. Chem. 252*, 1852−1857.
52. Erez, T., Gdalevsky, G. Y., Torchinsky, Y. M., Phillips, R. S., and Parola, A. H. (1998) Cold inactivation and dissociation into dimers of *Escherichia coli* tryptophanase and its W330F mutant form, *Biochim. Biophys. Acta 1384*, 365−372.
53. Schneider, T. R. (2002) A genetic algorithm for the identification of conformationally invariant regions in protein molecules, *Acta Crystallogr., Sect. D 58*, 195−208.
54. Kiick, D. M., and Phillips, R. S. (1988) Mechanistic deductions from kinetic isotope effects and pH studies of pyridoxal phosphate dependent carbon−carbon lyases: *Erwinia herbicola* and *Citrobacter freundii* tyrosine phenol-lyase, *Biochemistry 27*, 7333−7338.
55. Demidkina, T. V., Myagkikh, I. V., Antson, A. A., and Harutyunyan, E. H. (1988) Crystallization and crystal data on tyrosine phenol-lyase, *FEBS Lett. 232*, 381−382.

BI0601858